

Communication

# Symmetrical Noncovalent Interactions Br $\cdots$ Br Observed in Crystal Structure of Exotic Primary Peroxide

Dmitrii S. Bolotin <sup>1,\*</sup>, Mikhail V. Il'in <sup>1</sup>, Vitalii V. Suslonov <sup>2</sup> and Alexander S. Novikov <sup>1,\*</sup> 

<sup>1</sup> Institute of Chemistry, Saint Petersburg State University, Universitetskaya Nab. 7/9, Saint Petersburg 199034, Russia; ilinmichail21@gmail.com

<sup>2</sup> Center for X-ray Diffraction Studies, Saint Petersburg State University, Universitetskii Pr., 26, Saint Petersburg 198504, Russia; v.suslonov@spbu.ru

\* Correspondence: d.s.bolotin@spbu.ru (D.S.B.); a.s.novikov@spbu.ru (A.S.N.)

Received: 31 March 2020; Accepted: 14 April 2020; Published: 17 April 2020



**Abstract:** 4-Bromobenzamidrazone reacts with cyclopentanone giving 3-(4-bromophenyl)-5-(4-peroxobutyl)-1,2,4-triazole, which precipitated as pale-yellow crystals during the reaction. The intermolecular noncovalent interactions Br $\cdots$ Br in the single-crystal XRD structure of the peroxy compound were studied theoretically using quantum chemical calculations ( $\omega$ B97XD/x2c-TZVPall) and quantum theory of atoms in molecules (QTAIM) analysis. These attractive intermolecular noncovalent interactions Br $\cdots$ Br is type I halogen $\cdots$ halogen contacts and their estimated energy is 2.2–2.5 kcal/mol. These weak interactions are suggested to be one of the driving forces (albeit surely not the main one) for crystallization of the peroxy compound during the reaction and thus its stabilization in the solid state.

**Keywords:** organic peroxide; triazole; DFT; QTAIM; noncovalent interactions; halogen bonding

## 1. Introduction

Short halogen $\cdots$ halogen contacts can be classified on two types (Figure 1) [1]. Type I is simply due to crystal packing effects, while type II (halogen bonding) is directed noncovalent interactions [2] formed between the  $\sigma$ -hole (electrophilic region) on the halogen (Hal) atom and a nucleophile.

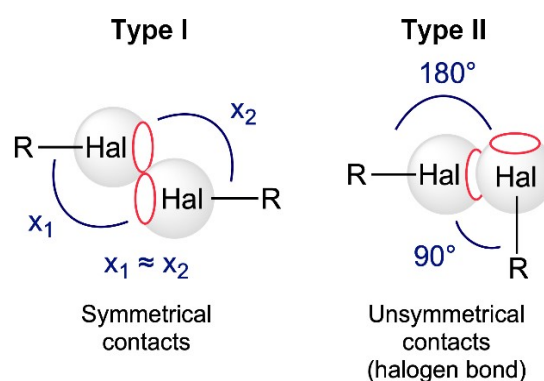


**Figure 1.** Types of Hal $\cdots$ Hal noncovalent interactions.

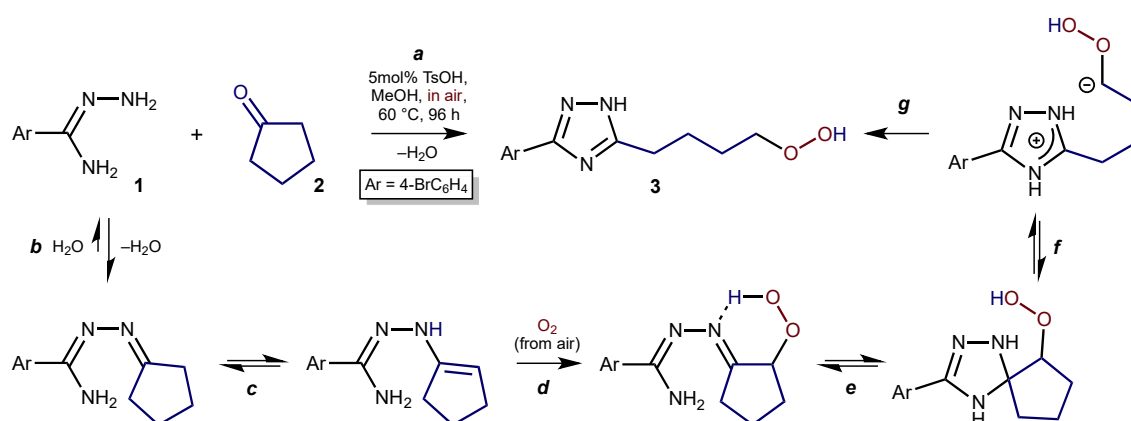
Although both types of Hal $\cdots$ Hal contacts have similar abundance, today halogen bond (type II) has drawn significantly higher attention and similarly to hydrogen bonds, metallophilic contacts, and stacking interactions, halogen bonding is now widely used in crystal growth and design and in

supramolecular engineering [1,3–5]. The recently published relevant reviews are devoted to theoretical approaches to Hal...Hal contacts [6,7] and also application of Hal...Hal contacts in supramolecular engineering [8–12], catalytic reactions [13], organometallic and coordination chemistry [14–18], polymer science [19], medical chemistry and drug discovery [20–23], and to the involvement of Hal...Hal contacts in human function [24].

In this communication, we describe symmetrical type I noncovalent interactions observed between two bromine atoms, which allow isolation of primary peroxide formed in the reaction of amidrazone and cyclopentanone (along with different hydrogen bonds and other crystal packing effects dominating in this respect).

## 2. Results and Discussion

Reaction of 4-bromobenzamidrazone **1** with cyclopentanone **2** (1.2 equiv.) in methanol at 60 °C for 96 h in air results in unpredictable formation of 1,2,4-triazole **3** featuring aliphatic peroxide chain as several pale-yellow crystals, which were studied by single-crystal XRD (Scheme 1a and Figure 2), among the formation of 1,4-di(4-bromophenyl)tetrazine as a major product of the reaction [25]. Reaction of other *para*-substituted aromatic amidrazones, i.e., 4-RC<sub>6</sub>H<sub>4</sub>C(NH<sub>2</sub>)=NNH<sub>2</sub> (R = CF<sub>3</sub>, H, MeO) under the same conditions resulted in formation of only the corresponding tetrazines [25], whereas generation of the peroxide substrates was not observed even by HRESI<sup>+</sup>-MS.



**Scheme 1.** Reaction scheme of the formation of primary aliphatic peroxide (a) and the plausible mechanism of its generation (b–g).

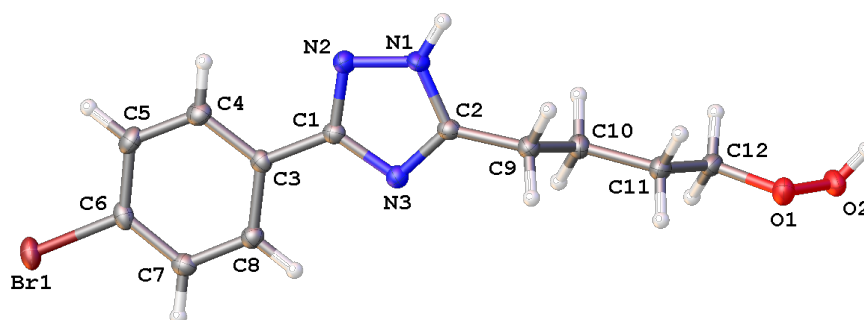


**Figure 2.** The single-crystal XRD structure of **3**. Probability level of thermal ellipsoids—50%.

Plausible mechanism of this reaction includes an acid catalyzed reversible Schiff condensation (b). <sup>1</sup>H NMR reaction monitoring in CD<sub>3</sub>OD reveals that the reaction mixture approached an equilibrium (molar ratio 1:3 ≈ 1:9) at 60 °C for ca. 1 h. The reaction stops at this step in the case of utilization of an argon atmosphere, but under air it proceeds further and the next plausible step includes tautomerization (c) and oxidation of the enamine by molecular oxygen giving secondary peroxide (d). Availability of electron-withdrawing peroxy group close to the imine C atom provides intramolecular nucleophilic

attack by the  $\text{NH}_2$  moiety giving spiro intermediate (e). The last step includes heterolytic C–C bond splitting, which accompanied by aromatization of the 1,2,4-triazole cycle and stabilization of the carbanion by the electron-withdrawing peroxy group (f). Proton transfer from the N atom to the C atom terminates the reaction (g). Further experimental or computational studies are needed to confirm the suggested mechanism.

Because precipitation of the peroxy compound **3** has been observed only in the case of amidrazone **1** featuring bromine atom in the structure, which (i) has intermediate electronic effects in the row of R's:  $\text{CF}_3$ , Br, H, MeO, and (ii) cannot sterically affect the reaction proceeding, we suggested that weak halogen...halogen intermolecular interactions (along with different hydrogen bonds and other crystal packing effects dominating in this respect) provide precipitation of **3** during the reaction progress and thus stabilization the peroxide **3** in the solid state. Based upon this observation and our interest in unusual noncovalent interactions involving halogen atoms, we studied theoretically the origin of the symmetrical intermolecular  $\text{Br}\cdots\text{Br}$  contacts (type I, Figure 1), which were detected in the single-crystal XRD structure of **3**.

Indeed, the intermolecular distance  $\text{Br}\cdots\text{Br}$  in the crystal structure of **3** is 3.414 Å, which is shorter than the sum of van der Waals radii [26] of two bromine atoms (3.66 Å). In order to confirm from a theoretical viewpoint the existence of these intermolecular short contacts  $\text{Br}\cdots\text{Br}$  in the crystal under study, we carried out quantum chemical calculations ( $\omega\text{B97XD}/\text{x2c-TZVPP}$  level) and quantum theory of atoms in molecules (QTAIM) analysis [27] for model dimeric associate (Table 1). The visualization of intermolecular noncovalent interactions  $\text{Br}\cdots\text{Br}$  in the crystal structure of **3** are shown in Figures 3 and 4.

**Table 1.** Results of quantum theory of atoms in molecules (QTAIM) analysis:  $\rho(\mathbf{r})$ ,  $\nabla^2\rho(\mathbf{r})$ ,  $\lambda_2$ ,  $H_b$ ,  $V(\mathbf{r})$ , and  $G(\mathbf{r})$  values (in a.u.) at the bond critical point, corresponding to intermolecular noncovalent interactions  $\text{Br}\cdots\text{Br}$  in the single-crystal XRD structure of **3** and estimated energy for these contacts defined by two approaches— $E_{\text{int}}$  (kcal/mol).

Density of All Electrons $\rho(\mathbf{r})$	Laplacian of Electron Density $\nabla^2\rho(\mathbf{r})$	$\lambda_2$	Energy Density $H_b$	Potential Energy Density $V(\mathbf{r})$	Lagrangian Kinetic Energy $G(\mathbf{r})$	$E_{\text{int}}^a$	$E_{\text{int}}^b$
0.010	0.034	-0.012	0.001	-0.006	0.007	2.2	2.5

<sup>a</sup>  $E_{\text{int}} = 0.58(-V(\mathbf{r}))$  [28]; <sup>b</sup>  $E_{\text{int}} = 0.57G(\mathbf{r})$  [28].

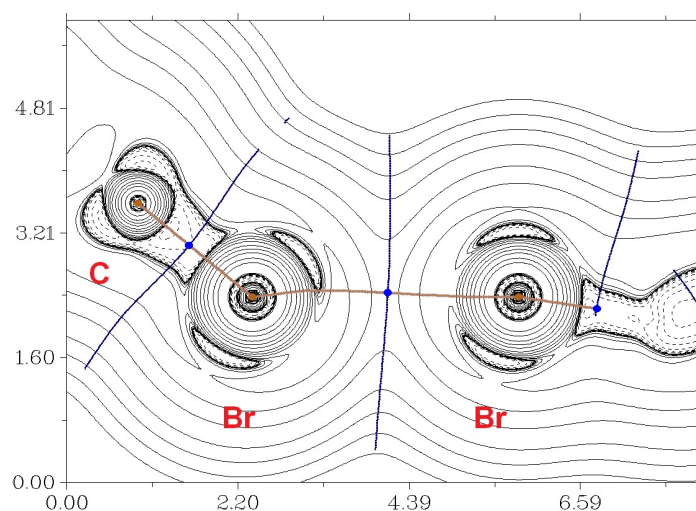


**Figure 3.** Visualization of intermolecular noncovalent interactions  $\text{Br}\cdots\text{Br}$  in the single-crystal XRD structure of **3** (distribution of the Laplacian of electron density  $\nabla^2\rho(\mathbf{r})$ , bond paths and selected zero-flux surfaces, length units—Å).

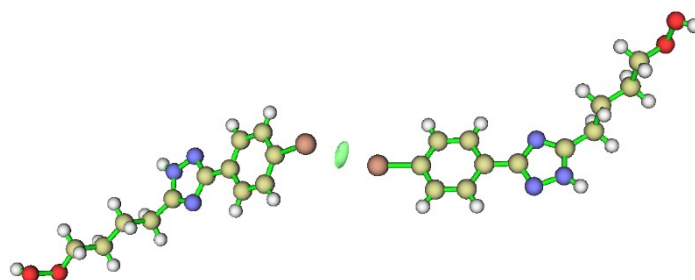


**Figure 4.** Visualization of intermolecular noncovalent interactions Br...Br in the single-crystal XRD structure of **3** using the independent gradient model analysis based on promolecular density (high quality grid, ~1728000 points in total; value of isosurface = 0.01,  $\delta g^{\text{inter}}$  descriptor).

The appropriate bond critical point for intermolecular noncovalent interactions Br...Br in the single-crystal XRD structure of **3** was found during the QTAIM analysis. The properties of electron density in this bond critical point are typical for noncovalent interactions [29,30] and, in particular, for similar weak contacts halogen...halogen [31–33]. Energy for these contacts (2.2–2.5 kcal/mol) was estimated using the procedures developed by Tsirelson et al. for non-covalent contacts involving bromine atoms using the equations  $E_{\text{int}} = 0.58(-V(\mathbf{r}))$  or  $E_{\text{int}} = 0.57G(\mathbf{r})$ , respectively [28]. Note that estimated energy of these symmetrical intermolecular Br...Br contacts in the single-crystal XRD structure of **3** is very well consistent with the approximate dimerization energy of the appropriated model dimeric associate calculated at the  $\omega\text{B97XD}/\text{x2c-TZVPall}$  level (stabilization amounts to 2.1 kcal/mol). The balance between  $G(\mathbf{r})$  and  $V(\mathbf{r})$  at the bond critical point reveals that a covalent contribution in the intermolecular noncovalent interactions Br...Br in the X-ray structure of **3** is negligible [34]. The sign of  $\lambda_2$  in appropriate bond critical point for intermolecular noncovalent interactions Br...Br in the X-ray structure of **3** reveals that these contacts are attractive [35,36].

### 3. Materials and Methods

#### 3.1. Synthetic Procedure

A solution of amidrazone **1** (214 mg, 1 mmol), TsOH·H<sub>2</sub>O (10 mg, 0.05 mmol), and cyclopentanone **2** (100 mg, 1.2 mmol) in methanol (5 mL) was kept at 60 °C for 96 h. The crystals of **3** formed during the reaction were isolated from the reaction solution and were subjected to single-crystal XRD.

#### 3.2. X-Ray Diffraction Study

The Agilent Technologies «Xcalibur» diffractometer was used for X-ray diffraction experiment. X-ray diffraction experiment was collected at 100 K using monochromated MoK $\alpha$  radiation. The parameters of unit cell (Table S1) were refined by least square techniques in the  $2\theta$  range of 5–55° for MoK $\alpha$ . Structure was solved using Superflip [37,38] by the charge flipping method and refined using the SHELXL [39] program implemented in the OLEX2 [40] program package. The CrysAlisPro [41] program complex was used for empirical absorption correction using spherical harmonics in SCALE3 ABSPACK scaling algorithm. The crystallographic data have been deposited at Cambridge Crystallographic Data Centre (CCDC 1969513) and can be obtained free of charge via [www.ccdc.cam.ac.uk/data\\_request/cif](http://www.ccdc.cam.ac.uk/data_request/cif). Also appropriated cif-file with single-crystal XRD structure of **3** is given in Supplementary Materials.

#### 3.3. Computational Details

The single point DFT calculations based on the experimental X-ray geometry of model dimeric associate were carried out using the dispersion-corrected hybrid functional  $\omega\text{B97XD}$  [42] in Gaussian-09 [43] program package. The segmented contracted all-electron relativistic triple- $\zeta$  valence quality basis sets x2c-TZVPPall [44] were used. The quantum theory of atoms in molecules (QTAIM) analysis [27] and independent gradient model analysis of noncovalent interactions based on

promolecular density [45] were performed in Multiwfn program package (v. 3.6) [46]. The Cartesian atomic coordinates for model dimeric associate are presented in Table S2 (Supporting Information).

#### 4. Conclusions

In this work, the formation of organic primary peroxide from amidrazone and cyclopentanone was described. The 3-(4-bromophenyl)-5-(4-peroxobutyl)-1,2,4-triazole precipitates as pale-yellow crystals during the reaction and the intermolecular noncovalent interactions Br $\cdots$ Br in the crystal structure were determined. Results of quantum chemical calculations indicated that these attractive intermolecular noncovalent interactions Br $\cdots$ Br is type I halogen $\cdots$ halogen contacts and their estimated energy is 2.2–2.5 kcal/mol. These symmetric weak interactions (along with different hydrogen bonds and other crystal packing effects) are suggested to be one of the driving forces for crystallization of the peroxo compound during the reaction and thus its stabilization in the solid state. Further studies of the found reaction are under investigation in our group.

**Supplementary Materials:** The following Supporting Information is available online at <http://www.mdpi.com/2073-8994/12/4/637/s1>, Table S1: Crystal data for **3**, Table S2: Cartesian atomic coordinates for model dimeric associate of **3**, cif-file with single-crystal XRD structure of **3**.

**Author Contributions:** Conceptualization, D.S.B. and A.S.N.; methodology, D.S.B., M.V.I., V.V.S. and A.S.N.; software, A.S.N.; validation, D.S.B., M.V.I., V.V.S. and A.S.N.; formal analysis, D.S.B., M.V.I., V.V.S. and A.S.N.; investigation, D.S.B., M.V.I., V.V.S. and A.S.N.; resources, D.S.B., M.V.I., V.V.S. and A.S.N.; data curation, D.S.B. and A.S.N.; writing—original draft preparation, D.S.B. and A.S.N.; writing—review and editing, D.S.B., M.V.I., V.V.S. and A.S.N.; visualization, D.S.B. and A.S.N.; supervision, D.S.B. and A.S.N.; project administration, D.S.B. and A.S.N.; funding acquisition, D.S.B. All authors have read and agreed to the published version of the manuscript.

**Funding:** This work was financially supported by Russian Science Foundation (grant 17-73-20004).

**Acknowledgments:** Physicochemical studies were performed at the Center for X-ray Diffraction Studies belonging to Saint Petersburg State University. We thank the Reviewers of this communication for their valuable advices and comments.

**Conflicts of Interest:** The authors declare no conflict of interest. The funders had no role in the design of the study; in the collection, analyses, or interpretation of data; in the writing of the manuscript, or in the decision to publish the results.

#### References

1. Cavallo, G.; Metrangolo, P.; Milani, R.; Pilati, T.; Priimagi, A.; Resnati, G.; Terraneo, G. The Halogen Bond. *Chem. Rev.* **2016**, *116*, 2478–2601. [[CrossRef](#)]
2. Alkorta, I.; Elguero, J.; Frontera, A. Not Only Hydrogen Bonds: Other Noncovalent Interactions. *Crystals* **2020**, *10*, 180. [[CrossRef](#)]
3. Metrangolo, P.; Meyer, F.; Pilati, T.; Resnati, G.; Terraneo, G. Halogen Bonding in Supramolecular Chemistry. *Chem. Rev.* **2015**, *115*, 7118–7195. [[CrossRef](#)]
4. Wang, H.; Wang, W.; Jin, W.J.  $\sigma$ -Hole Bond vs  $\pi$ -Hole Bond: A Comparison Based on Halogen Bond. *Chem. Rev.* **2016**, *116*, 5072–5104. [[CrossRef](#)] [[PubMed](#)]
5. Mukherjee, A.; Tothadi, S.; Desiraju, G.R. Halogen bonds in crystal engineering: Like hydrogen bonds yet different. *Acc. Chem. Res.* **2014**, *47*, 2514–2524. [[CrossRef](#)] [[PubMed](#)]
6. Politzer, P.; Murray, J. An Overview of Strengths and Directionalities of Noncovalent Interactions:  $\sigma$ -Holes and  $\pi$ -Holes. *Crystals* **2019**, *9*, 165. [[CrossRef](#)]
7. Seth, S.K.; Bauza, A.; Frontera, A. Quantitative Analysis of Weak Non-covalent  $\sigma$ -Hole and  $\pi$ -Hole Interactions. *Underst. Intermol. Interact. Solid State Approaches Tech.* **2019**, *26*, 285–333.
8. Li, B.; Zang, S.Q.; Wang, L.Y.; Mak, T.C. Halogen bonding: A powerful, emerging tool for constructing high-dimensional metal-containing supramolecular networks. *Coord. Chem. Rev.* **2016**, *308*, 1–21. [[CrossRef](#)]
9. Maharramov, A.M.; Mahmudov, K.T.; Kopylovich, M.N.; Pombeiro, A.J. *Non-Covalent Interactions in the Synthesis and Design of New Compounds*; Wiley Online Library: Hoboken, NJ, USA, 2016.
10. Wang, W.M.; Li, X.Z.; Zhang, L.; Chen, J.L.; Wang, J.H.; Wu, Z.L.; Cui, J.Z. A series of [2  $\times$  2] square grid LnIII<sub>4</sub> clusters: A large magnetocaloric effect and single-molecule-magnet behavior. *New J. Chem.* **2019**, *43*, 7419–7426. [[CrossRef](#)]

11. Tepper, R.; Schubert, U.S. Halogen Bonding in Solution: Anion Recognition, Templated Self-Assembly, and Organocatalysis. *Angew. Chem. Int. Ed.* **2018**, *57*, 6004–6016. [[CrossRef](#)]
12. Brammer, L.; Espallargas, G.M.; Libri, S. Combining metals with halogen bonds. *CrystEngComm* **2008**, *10*, 1712–1727. [[CrossRef](#)]
13. Mahmudov, K.T.; Gurbanov, A.V.; Guseinov, F.I.; da Silva, M.F.C.G. Noncovalent interactions in metal complex catalysis. *Coord. Chem. Rev.* **2019**, *387*, 32–46. [[CrossRef](#)]
14. Mahmudov, K.T.; Arimitsu, S.; Saá, J.M.; Sarazin, Y.; Frontera, A.; Yamada, S.; Caminade, A.M.; Chikkali, S.H.; Mal, P.; Momiyama, N.; et al. *Noncovalent Interactions in Catalysis*; Royal Society of Chemistry: London, UK, 2019.
15. Nagorny, P.; Sun, Z.K. New approaches to organocatalysis based on C-H and C-X bonding for electrophilic substrate activation. *Beilstein J. Org. Chem.* **2016**, *12*, 2834–2848. [[CrossRef](#)] [[PubMed](#)]
16. Mahmudov, K.T.; Kopylovich, M.N.; da Silva, M.F.C.G.; Pombeiro, A.J. Non-covalent interactions in the synthesis of coordination compounds: Recent advances. *Coord. Chem. Rev.* **2017**, *345*, 54–72. [[CrossRef](#)]
17. Benz, S.; Poblador-Bahamonde, A.I.; Low-Ders, N.; Matile, S. Catalysis with Pnictogen, Chalcogen, and Halogen Bonds. *Angew. Chem. Int. Ed.* **2018**, *57*, 5408–5412. [[CrossRef](#)]
18. Breugst, M.; von der Heiden, D.; Schmauck, J. Novel Noncovalent Interactions in Catalysis: A Focus on Halogen, Chalcogen, and Anion- $\pi$  Bonding. *Synthesis* **2017**, *49*, 3224–3236. [[CrossRef](#)]
19. Berger, G.; Soubhye, J.; Meyer, F. Halogen bonding in polymer science: From crystal engineering to functional supramolecular polymers and materials. *Polym. Chem.* **2015**, *6*, 3559–3580. [[CrossRef](#)]
20. Mendez, L.; Henriquez, G.; Sirimulla, S.; Narayan, M. Looking Back, Looking Forward at Halogen Bonding in Drug Discovery. *Molecules* **2017**, *22*, 1397. [[CrossRef](#)]
21. Ho, P.S. Halogen bonding in medicinal chemistry: From observation to prediction. *Future Med. Chem.* **2017**, *9*, 637–640. [[CrossRef](#)]
22. Dalpiaz, A.; Pavan, B.; Ferretti, V. Can pharmaceutical co-crystals provide an opportunity to modify the biological properties of drugs? *Drug Discov. Today* **2017**, *22*, 1134–1138. [[CrossRef](#)]
23. Lu, Y.; Liu, Y.; Xu, Z.; Li, H.; Liu, H.; Zhu, W. Halogen bonding for rational drug design and new drug discovery. *Exp. Opin. Drug. Dis.* **2012**, *7*, 375–383. [[CrossRef](#)] [[PubMed](#)]
24. Bayse, C.A. Halogen bonding from the bonding perspective with considerations for mechanisms of thyroid hormone activation and inhibition. *New J. Chem.* **2018**, *42*, 10623–10632. [[CrossRef](#)] [[PubMed](#)]
25. Burianova, V.K.; Bolotin, D.S.; Mikhherdov, A.S.; Novikov, A.S.; Mokolokolo, P.P.; Roodt, A.; Boyarskiy, V.P.; Dar'in, D.; Krasavin, M.; Suslonov, V.V.; et al. Mechanism of generation of closo-decaborato amidrazones. Intramolecular non-covalent B–H $\cdots\pi$ (Ph) interaction determines stabilization of the configuration around the amidrazone C=N bond. *New J. Chem.* **2018**, *42*, 8693–8703. [[CrossRef](#)]
26. Bondi, A. van der Waals volumes and radii. *J. Phys. Chem.* **1964**, *68*, 441–451. [[CrossRef](#)]
27. Bader, R.F.W. *Atoms in Molecules: A Quantum Theory*; Oxford University Press: Oxford, UK, 1990.
28. Bartashevich, E.V.; Tsirelson, V.G. Interplay between non-covalent interactions in complexes and crystals with halogen bonds. *Russ. Chem. Rev.* **2014**, *83*, 1181–1203. [[CrossRef](#)]
29. Mikhherdov, A.S.; Kinzhalov, M.A.; Novikov, A.S.; Boyarskiy, V.P.; Boyarskaya, I.A.; Avdontceva, M.S.; Kukushkin, V.Y. Ligation-Enhanced  $\pi$ -Hole $\cdots\pi$  Interactions Involving Isocyanides: Effect of  $\pi$ -Hole $\cdots\pi$  Noncovalent Bonding on Conformational Stabilization of Acyclic Diaminocarbene Ligands. *Inorg. Chem.* **2018**, *57*, 6722–6733. [[CrossRef](#)] [[PubMed](#)]
30. Kolari, K.; Sahamies, J.; Kalenius, E.; Novikov, A.S.; Kukushkin, V.Y.; Haukka, M. Metallophilic interactions in polymeric group 11 thiols. *Solid State Sci.* **2016**, *60*, 92–98. [[CrossRef](#)]
31. Adonin, S.A.; Gorokh, I.D.; Novikov, A.S.; Abramov, P.A.; Sokolov, M.N.; Fedin, V.P. Halogen Contacts-Induced Unusual Coloring in BiIII Bromide Complex: Anion-to-Cation Charge Transfer via Br $\cdots$ Br Interactions. *Chem.—Eur. J.* **2017**, *23*, 15612–15616. [[CrossRef](#)]
32. Adonin, S.A.; Udalova, L.I.; Abramov, P.A.; Novikov, A.S.; Yushina, I.V.; Korolkov, I.V.; Semitut, E.Y.; Derzhavskaya, T.A.; Stevenson, K.J.; Troshin, P.A.; et al. A Novel Family of Polyiodo-Bromoantimonate(III) Complexes: Cation-Driven Self-Assembly of Photoconductive Metal-Polyhalide Frameworks. *Chem.—Eur. J.* **2018**, *24*, 14707–14711. [[CrossRef](#)]
33. Adonin, S.A.; Bondarenko, M.A.; Novikov, A.S.; Abramov, P.A.; Plyusnin, P.E.; Sokolov, M.N.; Fedin, V.P. Halogen bonding-assisted assembly of bromoantimonate(v) and polybromide-bromoantimonate-based frameworks. *CrystEngComm* **2019**, *21*, 850–856. [[CrossRef](#)]

34. Espinosa, E.; Alkorta, I.; Elguero, J.; Molins, E. From weak to strong interactions: A comprehensive analysis of the topological and energetic properties of the electron density distribution involving X–H···F–Y systems. *J. Chem. Phys.* **2002**, *117*, 5529–5542. [[CrossRef](#)]
35. Johnson, E.R.; Keinan, S.; Mori-Sánchez, P.; Contreras-García, J.; Cohen, A.J.; Yang, W. Revealing Noncovalent Interactions. *J. Am. Chem. Soc.* **2010**, *132*, 6498–6506. [[CrossRef](#)]
36. Contreras-García, J.; Johnson, E.R.; Keinan, S.; Chaudret, R.; Piquemal, J.P.; Beratan, D.N.; Yang, W. NCIPlot: A program for plotting non-covalent interaction regions. *J. Chem. Theory Comput.* **2011**, *7*, 625–632. [[CrossRef](#)] [[PubMed](#)]
37. Palatinus, L.; Chapuis, G. SUPERFLIP. A computer program for the solution of crystal structures by charge flipping in arbitrary dimensions. *J. Appl. Cryst.* **2007**, *40*, 786–790. [[CrossRef](#)]
38. Palatinus, L.; Prathapa, S.J.; van Smaalen, S. EDMA: A computer program for topological analysis of discrete electron densities. *J. Appl. Cryst.* **2012**, *45*, 575–580. [[CrossRef](#)]
39. Sheldrick, G.M. Crystal structure refinement with SHELXL. *Acta Cryst.* **2015**, *C71*, 3–8.
40. Dolomanov, O.V.; Bourhis, L.J.; Gildea, R.J.; Howard, J.A.; Puschmann, H. OLEX2: A complete structure solution, refinement and analysis program. *J. Appl. Cryst.* **2009**, *42*, 339–341. [[CrossRef](#)]
41. *CrysAlisPro*; Version 1.171.36.32; Agilent Technologies: Santa Clara, CA, USA, 8 February 2013.
42. Chai, J.D.; Head-Gordon, M. Long-range corrected hybrid density functionals with damped atom-atom dispersion corrections. *Phys. Chem. Chem. Phys.* **2008**, *10*, 6615–6620. [[CrossRef](#)]
43. Frisch, M.J.; Trucks, G.W.; Schlegel, H.B. *Gaussian 09, Revision C.01*; Gaussian, Inc.: Wallingford, CT, USA, 2010.
44. Pollak, P.; Weigend, F. Segmented Contracted Error-Consistent Basis Sets of Double- and Triple-zeta Valence Quality for One- and Two-Component Relativistic All-Electron Calculations. *J. Chem. Theory Comput.* **2017**, *13*, 3696–3705. [[CrossRef](#)]
45. Lefebvre, C.; Rubez, G.; Khartabil, H.; Boisson, J.C.; Contreras-García, J.; Hénon, E. Accurately extracting the signature of intermolecular interactions present in the NCI plot of the reduced density gradient versus electron density. *Phys. Chem. Chem. Phys.* **2017**, *19*, 17928–17936. [[CrossRef](#)]
46. Lu, T.; Chen, F. Multiwfn: A multifunctional wavefunction analyzer. *J. Comput. Chem.* **2012**, *33*, 580–592. [[CrossRef](#)] [[PubMed](#)]



© 2020 by the authors. Licensee MDPI, Basel, Switzerland. This article is an open access article distributed under the terms and conditions of the Creative Commons Attribution (CC BY) license (<http://creativecommons.org/licenses/by/4.0/>).